# A simple model for multi-ion permeation

## Single-vacancy conduction in a simple pore model

Mark F. Schumaker and Roderick MacKinnon

Department of Chemistry, Brandeis University, Waltham, Massachusetts 02254; and Department of Cellular and Molecular Physiology, Harvard Medical School, Boston, Massachusetts 02115 USA

ABSTRACT Recent experimental evidence suggests that certain membrane channels operate in a nearly ion-saturated state. We therefore consider a "single-vacancy" model of ion permeation: if a channel has $n$ conducting sites, it will contain either $n$ or $n - 1$ ions. Simple analytical expressions for the current, conductance, and reversal potential under bi-ionic conditions are derived. The results are compared with those of single ion models and recent experiments on $Ca^{2+}$- activated $K^+$ channels.

## INTRODUCTION

In 1955 Hodgkin and Keynes demonstrated that K ions diffuse through the membrane of the cuttle fish giant axon in a single-file, "coupled" fashion (Hodgkin and Keynes, 1955). Since then, similar experiments have repeatedly confirmed that $K^+$ channels from many different membranes are multi-ion pores, in some cases holding at least three K ions simultaneously (Horowicz et al., 1968; Begenisich and DeWeer, 1980; Spalding et al., 1981). Furthermore, electrophysiological studies have provided strong evidence that other ion channels, including $Ca^{2+}$ and $Na^+$ channels, can hold more than one ion (Almers and McCleskey, 1984; Hess and Tsien, 1984; Fukushima and Hagiwara, 1985; Chandler and Meues, 1965; Cahalan and Begenisich, 1976). Recently, certain ion channels have been shown to display a rather surprising multi-ion property; their conduction pores appear to have multiple high-affinity ion binding sites. One example is the $Ca^{2+}$-activated $K^+$ channel from red blood cells (Gárdos, 1958). The flux-ratio exponent for this channel is ~2.7, over a range of $K^+$ concentrations (intracellular 145–30 mM, extracellular 150–1 mM; Vestergaard-Bogind et al., 1985; Stampe, P., personal communication). The result demonstrates that as the ion activity is lowered the occupancy of the conduction pore remains high; the pore does not become ion-depleted as one might expect. Another example of an "ion-avid" channel is the mammalian skeletal muscle $Ca^{2+}$-activated $K^+$ channel, which has at least three ions in its pore, even when the conducting ion concentration is lowered to 10 mM (Neyton and Miller, 1988).[1] These channels appear to operate in a nearly ion-saturated state, and this realization has compelled us to investigate a model for ion conduction in such ion-filled channels. In this paper we consider a "single-vacancy" model of ion permeation: if a channel has $n$ conduction sites, we allow it to contain either $(n - 1)$ or $n$ ions. If an ion channel has charged or polar groups in its conduction pathway, which must be electrically neutralized by conduction counter-ions, then the single vacancy restriction imposed by the model is realistic.

Single-vacancy conduction is one of the two limits of discrete state models that allow easy analytical investigation, the other being the single-ion limit, which has been thoroughly investigated by Läuger (1973). A similar vacancy conduction mechanism was previously considered by Kohler and Heckmann (1979) in an analysis of the flux ratio exponent. Here we investigate the current, conductance and bi-ionic reversal potential for single-vacancy conduction. By considering a special case, analogous to the "simple pore model" of Läuger, we are able to derive analytical expressions which are simple enough to be readily grasped. The aim of this study is not to generate expressions for the purpose of fitting experimental data, but rather to gain some general, qualitative insights into a conduction mechanism, which may be operating in a class of ion channels, the $Ca^{2+}$-activated $K^+$ channels.

## THE MODEL

In Fig. 1 *a* an ion channel is portrayed as a series of potential energy barriers, which surround wells. The wells represent localized sites within the pore at which conducting ions sit. Ions hop from site to site and must pass through relatively energetic transition states in between. The channel with $n$ sites will contain either $n$ or $(n - 1)$ ions. We assume that ionic motions are not concerted; only one ion hops at a time. In analogy to the "simple pore model" of Läuger, we assume that the free-energy profile

Dr. Schumaker's present address is Department of Pure and Applied Mathematics, Washington State University, Pullman, Washington 99164.



0006-3495/90/10/975/10 $2.00

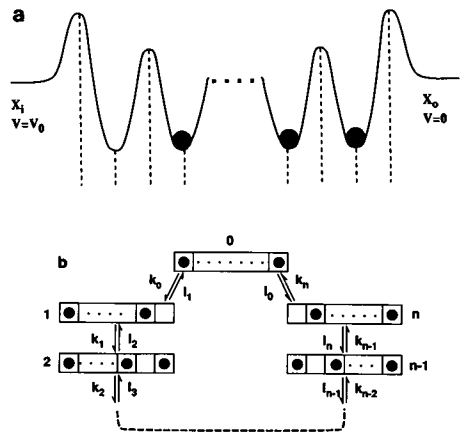


FIGURE 1 (*a*) Potential energy diagram for the simple pore model of a single-vacancy channel. The channel sits in a membrane between the "inside" and the "outside" reservoirs of electrolyte. Activities of permeant ions in these two reservoirs are $x_i$ and $x_o$, respectively. The electrical potential on the outside is $V = 0$ by definition; the electrical potential on the inside is $V = V_0$. (*b*) State diagram for the single-vacancy conduction mechanism. Numerals 0 through $n$ label states. Solid circles depict ions occupying binding sites; each state has at most a single vacancy. The $k_i$ and $l_j$ are rate constants for transitions counterclockwise and clockwise around the loop, respectively.

is symmetric and that, for a given ionic species, all wells have the same affinity and internal barriers have the same height, as is depicted in the figure (Läuger, 1973). Further, the barriers and wells are assumed to be evenly spaced in units of electrical distance. This model might correspond to a channel with a symmetrical conduction pathway whose ion binding sites are nearly identical, regularly spaced chemical groups. It is certainly an oversimplification of a real ion channel, but nevertheless enables us to investigate the qualitative properties of single-vacancy conduction, and that is the goal of this study.

The single-vacancy conduction model is a discrete state model, and the rate constants for the transition between states are assumed to have an exponential dependence on electrical potential. For this to give a reasonable approximation to the underlying microscopic motion of the ions, the height of the potential barriers must be at least several $k_BT$, where $k_B$ is Boltzmann's constant, and $T$ is the absolute temperature. The potential-energy profile must also provide clearly defined ion binding sites. Levitt (1986) and Cooper et al. (1988) discuss in more detail the assumptions implicit in discrete state models.

The assumption that ionic motions are not concerted deserves comment. The movement of an atom in a condensed phase has to be coupled to the movement of its neighboring atoms. This presents a problem for any multi-ion conduction model if non-concerted motion is assumed, because a vacancy is not a vacuum, it is the absence of an ion. One must therefore assume that water can slip by ions in the conduction pathway to fill a vacancy, or that the channel walls actually pinch off a vacancy.

## RESULTS AND DISCUSSION

### Flux equation

In this section we will derive an equation for the flux through an $n$-site single-vacancy pore in the presence of a single ionic species. The starting point for our analysis is the state diagram shown in Fig. 1 *b*. Each state is depicted as a schematic pore with occupied or unoccupied sites shown explicitly on either side and dots indicating occupied sites in between. State 0 is the completely filled state and all other states contain a single vacancy; the position of the vacancy determines the state of the system. Notice that this state diagram is topologically identical to the corresponding diagram for a single-ion channel, where state 0 would correspond to the empty channel, and the remaining states would be determined by the position of a single ion in the channel. In the single-ion model the transport of an ion across the membrane corresponds to the diffusion of an ion around the loop, whereas in the single vacancy model it corresponds to the diffusion of a vacancy around the loop. The close relationship between the state diagrams for single-vacancy and single-ion conduction will lead immediately to a simple connection between the flux equations for the two conduction mechanisms (see below).

When a state diagram has a very simple structure such as that shown in Fig. 1 *b*, with a small number of loops of connected states, it becomes very convenient to employ the King-Altman method to solve for the state probabilities and the fluxes around the loops (King and Altman, 1956). An extension of the method, called the cycle-flux technique (Hill, 1977), enables one to immediately write down an expression for the net flux of ions $J$ passing from the inside to the outside of the membrane:

$$J = D^{-1}(\pi^+ - \pi^-), \tag{1}$$

where $\pi^+$ is the product of the rate constants counterclockwise around the loop in the direction of the flux $J$ (see Fig. 1 *b*) and $\pi^-$ is the product of rate constants clockwise around the loop against the flux $J$:

$$\pi^+ = k_0 k_1 \ldots k_n \quad \text{and} \quad \pi^- = l_0 l_1 \ldots l_n. \tag{2}$$

The denominator $D$ is the sum of the directional diagrams $D_i$ (Hill, 1977); expressions for these are given in Appendix A. According to the simple pore model we fix the

following values for the rate constants:

$$k_0 = be^{\nu}, k_n = x_i ae^{\nu}, \quad \text{and} \quad k_i = ke^{\nu} \quad \text{for } i \in \{1, \ldots, n-1\},$$

$$l_0 = be^{-\nu}, l_1 = x_o ae^{-\nu}, \quad \text{and} \quad l_j = ke^{-\nu} \quad \text{for } j \in \{2, \ldots, n\}. \quad (3)$$

Thus, in the absence of a transmembrane potential, the (second-order) rate constant for an ion to enter the channel is $a$, the (first-order) rate constant for leaving the channel is $b$, and the (first-order) rate constant for hopping between sites within the channel is $k$. When an electrical potential $V_0$ is applied across the channel, rate constants are multiplied by the factor $e^{\nu}$ when ion movement is towards the outside reservoir, and by a factor $e^{-\nu}$ when ion movement is towards the inside reservoir. Here, $\nu$ is the dimensionless electrical potential difference between a well and the barrier to its right: $\nu = zeV_0/2(n+1)k_BT$, where $n$ is the number of ion binding sites, $z$ is the valence of the permeant ion and $e$ is the elementary electric charge.

Using the rate constants defined in Eq. 3 we can find a formula for the flux of ions through the model pore in the important case of symmetrical concentrations $x_i = x_o \equiv x$; the major intermediate expressions are given in Appendix A. The result is:

$$J = \frac{2akbx \sinh \nu \sinh (n+1)\nu}{A \sinh (n+1)\nu + (B-A)\sinh (n-1)\nu}, \quad (4)$$

where

$$A = xak + kb + (n-1)xab \quad \text{and} \quad B = x^2a^2 + 2kb + (n-2)xab. \quad (5)$$

This is a remarkably simple form. Consider for a moment the case when $ax = k = b$, that is, when the zero-voltage entrance, internal hopping and exit rates are all equal: then $A = B$ and Eq. 4 simplifies to $J = [2k/(n+1)]\sinh[eV_0/2(n+1)k_BT]$. This leads to a superlinear $I$-$V$ curve, where the current $I$ is related to the flux $J$ through $I = zeJ$. As the number of ion binding sites $n$ increases, the current becomes smaller and the $I$-$V$ curve becomes more nearly linear over a fixed range of voltages. In general, when the entrance, internal hopping and exit rates are not equal, the current still becomes smaller as $n$ increases, but the $I$-$V$ curve is not necessarily linear; when the term$(B - A)$ is positive the $I$-$V$ curve becomes more superlinear and when it is sufficiently negative the $I$-$V$ curve can become sublinear. Fig. 2 shows the relationship between current and voltage according to Eqs. 4 and 5 for three different sets of rate constants.

The state diagram of Fig. 1 $b$ can be transformed into a state diagram for a single ion channel by filling empty ion binding sites and emptying the filled ones. To maintain the direction of flux, one must also flip the diagram about its vertical symmetry axis. In addition, the rate constants $k_0$ and $k_n$ must be exchanged, and the rate constants $l_0$ and $l_1$ as well. The relationship between the flux equation for single-vacancy and single-ion conduction is therefore simple: Eq. 4 becomes a formula for the flux through an $n$-site single-ion channel when $ax$ and $b$ in the Eqs. 5 are exchanged. Because the single-ion and single-vacancy currents have the same dependence on voltage, it is clearly impossible to distinguish between these two cases on the basis of a single $I$-$V$ curve. However, Eqs. 4 and 5 predict that the current will depend on the concentration of $x$ in a very different way for the two conduction mechanisms. We will now consider the concentration dependence of ion conduction through a single vacancy channel.

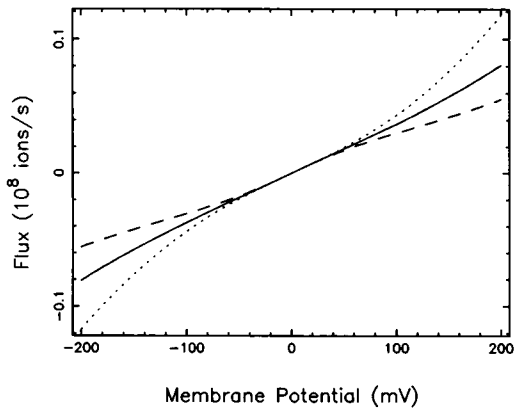


FIGURE 2 Three examples of flux $J$ as a function of voltage $V_0$. For the superlinear curve (*dotted line*): $ax = 1 \times 10^8\ s^{-1}$, $k = 2.26 \times 10^7\ s^{-1}$ and $b = 1.48 \times 10^7\ s^{-1}$. For the sublinear curve (*dashed line*): $ax = 1 \times 10^8\ s^{-1}$, $k = 1.02 \times 10^9\ s^{-1}$, and $b = 2.21 \times 10^6\ s^{-1}$. For the nearly linear curve (*solid line*): $ax = 1 \times 10^8\ s^{-1}$, $k = 1.21 \times 10^8\ s^{-1}$, and $b = 3.84 \times 10^6\ s^{-1}$. For each case there are $n = 3$ binding sites.

## Dependence of conductance on concentration

The conductance $\gamma$ at zero voltage and symmetric ion concentration may be calculated directly from Eq. 4 by differentiating: $\gamma = (\partial I/\partial V_0)_0$, where the final subscript 0 indicates $V_0 = 0$ and $x_i = x_o = x$. Alternatively, we may use

$$\left(\frac{\partial J}{\partial \nu}\right)_0 = \left(D^{-1}\frac{\partial(\pi^+ - \pi^-)}{\partial \nu}\right)_0, \quad (6)$$

which is obtained directly from Eq. 1 because $(\pi^+ - \pi^-)_0 = 0$ by detailed balance. $(D^{-1})_0$ may be easily

evaluated from Eq. A7. Either way, we obtain the result:

$$\gamma = \frac{z^2e^2}{k_BT}\frac{akbx}{[(n-1)ax+2k][ax+nb]} = \frac{z^2e^2}{k_BT}\frac{x}{A+Bx+Cx^2}, \quad (7)$$

where $A = 2na^{-1}$, $B = 2b^{-1} + (n-1)nk^{-1}$, and $C = (n-1)ak^{-1}b^{-1}$. Interchanging $ax$ and $b$ in Eq. 7 yields the formula for conductance through an $n$-site single-ion pore:

$$\gamma = \frac{z^2e^2}{k_BT}\frac{akb}{[2k+(n-1)b]}\frac{x}{(b+nax)}. \quad (8)$$

This agrees with the result previously found by Läuger (1973) for the simple pore model. Although the transformation connecting Eq. 7 to Eq. 8 is algebraically trivial, the resultant change in the dependence of $\gamma$ on $x$ is physically very significant. Whereas the conductance for the single ion model saturates with increasing symmetrical concentration $x$ in the characteristic fashion of a rectangular hyperboloid, Eq. 7 shows that for single-vacancy conduction the conductance reaches a maximum value at:

$$x^2_{max} = \frac{2nkb}{(n-1)a^2}, \quad (9)$$

and then decreases as $x$ is raised further. It is the quadratic term in the denominator of Eq. 7 that gives rise to this behavior. At low concentrations, when the quadratic term is small, $\gamma$ increases monotonically with $x$ as in the single ion model (Fig. 3) because the entrance rate is limited by the ion concentration. At higher concentrations, however, the quadratic term in the denominator will dominate and eventually cause the conductance to decrease with increasing $x$. A simple physical picture underlies this behavior. By inspecting the diagram in Fig. 1 *b* it is evident that at sufficiently high symmetric $x$, state 0 will become favored because the rate constants $l_1$ and $k_n$ are proportional to $x$. For example, when a channel is in state 0 and then an ion leaves (it undergoes a transition to state 1), large $x$ will favor the transition back to state 0: the channel becomes clogged. This reduces the frequency of cycles around the state diagram which is, in turn, proportional to the channel current.

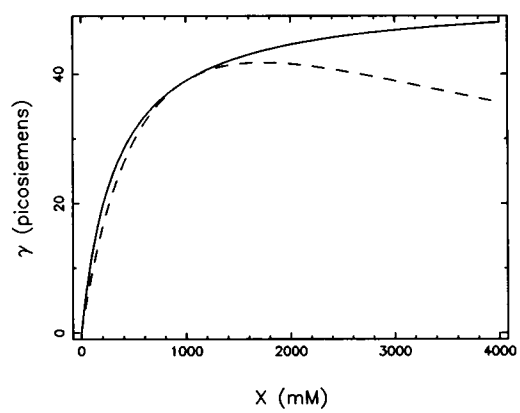


FIGURE 3 Comparison between single-ion conductance (*solid line*) and single-vacancy conductance (*dashed line*) as a function of symmetrical activity $x$. For both cases, rate constants are $a = 10^8\ s^{-1}\ M^{-1}$, $b = k = 10^8\ s^{-1}$. There are $n = 3$ ion binding sites.

The form of the conductance formula given to the right of the last equality in Eq. 7 holds for the general vacancy diffusion model, and not just for the simple pore model. This may be seen from Eq. 6, and illustrates the insight that may be obtained from analysis of state diagrams by means of the King-Altman method. The $x$ dependence in the denominator of Eq. 7 comes from the term $(D^{-1})_0$ in Eq. 6. $D$ is the sum of directional diagrams from Fig. 1 *b* and each directional diagram is a product of rate constants leading to a particular state. There are only two rate constants, $l_1$ and $k_n$, which give the rate of an ion entering the channel and are therefore proportional to $x$. The contribution of a directional diagram is then at most quadratic in $x$.

A conductance maximum has been demonstrated in gramicidin (Urban et al., 1978; Finkelstein and Andersen, 1981) and in a high-conductance $Ca^{2+}$-activated $K^+$ channel from skeletal muscle (Villarroel et al., 1988). In both of these cases, the maximum occurs at high $x_{max}$; ~1 M $Cs^+$ for gramicidin, and ~2 M $Rb^+$ for the $Ca^{2+}$-activated $K^+$ channel. These high $x_{max}$ values at first appear to be inconsistent with a single-vacancy conduction mechanism: if the pore is nearly saturated at low ion concentrations then clogging may occur at low concentrations. However, inspection of Eq. 9 leads to the conclusion that a high $x_{max}$ is entirely compatible with single-vacancy conduction. For example, if $a = 10^8\ M^{-1}s^{-1}$ (near the diffusion limit) and $k$ and $b$ are near $10^8 s^{-1}$ then $x_{max}$ will be close to 2 M for a three-ion channel.

Eq. 7 suggests a way to plot conductance data to distinguish between a single ion and a single-vacancy conductance mechanism. If one plots $x/\gamma$ as a function of $x$ the single-ion model predicts a straight line, whereas the single-vacancy model predicts a parabola: $x/\gamma = A + Bx + Cx^2$. In this way the clogging term $Cx^2$ can be identified as a deviation from linearity. The utility of this method for plotting the conductance data depends on the relative magitudes of the rate constants. For example, if $k$ and $b$ are equal, then for a three-site channel a 5% deviation from linearity will occur at $\frac{1}{3}x_{max}$. However, for $k/b$ much greater than or less than unity, the deviation from linearity (quadratic term) will remain unresolvable at concentrations even greater than $x_{max}$.

## Ion selectivity: reversal potential under bi-ionic conditions

A standard method of determining the relative permeability of two ions is to measure the zero-current or reversal potential when the inner solution is composed of one permeant species and the outer solution the other. In this section we investigate the predicted behavior of the reversal potential under these experimental conditions when ionic conduction occurs by a single vacancy mechanism. Consider two permeant ionic species, i and o. On the inside of the membrane, species i is present at activity $x_i$ and the activity of o is negligible. Correspondingly, on the outside species o has activity $x_o$ and the activity of i is negligible. One can therefore ignore the entry of i into the channel from the outside reservoir and vice versa. This, along with the condition that there can be at most a single vacancy in the channel at one time, implies the bi-ionic state diagram shown in Fig. 4. In the figure, filled circles represent ion i and enter the schematic pores from the left; open circles represent ion o and enter from the right. The only transition of an o ion into the inner reservoir is given by the unidirectional arrow connecting states N and M; this corresponds to the unidirectional flux $\overleftarrow{J}$. Similarly, the only transition of an ion i into the outer reservoir is given by the unidirectional arrow connecting states $-$N and $-$M, corresponding to the unidirectional flux $\overrightarrow{J}$. Unlike the situation where only a single permeant ionic species is present, there is a topological difference between the bi-ionic state diagrams for a single-vacancy and a single-ion channel. The bi-ionic state diagram for a single-ion channel has the shape of a figure 8, with the empty channel state connecting loops of states with a single open circle and a single filled circle.

To simplify calculations we again specialize to the case of a simple pore model. We assign for ion i a second-order rate constant $a_i$ for entrance into the channel, a first-order rate constant $k_i$ for transitions between sites within the channel, and a first-order rate constant $b_i$ for leaving the channel. Corresponding rate constants $a_o$, $k_o$, and $b_o$ are assigned to ion o. As before, the rates of outward transitions are multiplied by a factor $e^{\nu}$, and the rates of inward transitions are multiplied by the factor $e^{-\nu}$, where $\nu = eV_0/2(n+1)k_BT$.

The reversal potential $V_R$ is given implicitly by $\overleftarrow{J}(V_R) = \overrightarrow{J}(V_R)$. Detailed expressions for $\overleftarrow{J}$ and $\overrightarrow{J}$ in terms of the rate constants defined above are developed in Appendix B. Although it is not possible to solve analytically for $V_R$ in the general case, one can find the solution $\underline{V}_R$ in the limit of low concentrations $k_i \gg nx_ia_i$, and $k_o \gg nx_oa_o$, as well as the solution $\overline{V}_R$ in the limit of high concentrations $x_ia_i \gg k_i$ and $x_oa_o \gg k_o$. These limits are given by:

$$\underline{V}_R = \frac{k_BT}{ze}\left\{\ln\frac{x_o}{x_i} + \ln\frac{a_o}{a_i} + \frac{n-1}{n}\ln\frac{b_i}{b_o}\right\}, \qquad (10)$$

$$\overline{V}_R = \frac{k_BT}{ze}\left\{\ln\frac{x_o}{x_i} + \ln\frac{a_o}{a_i} + \frac{1}{n-1}\ln\frac{k_o}{k_i} + \ln\frac{b_i}{b_o}\right\}. \qquad (11)$$

Eqs. 10 and 11 indicate that the reversal potential can vary as the absolute ion activity changes even if the activity ratio $x_i/x_o$ is fixed (Fig. 5). $V_R$ approaches $\underline{V}_R$ in

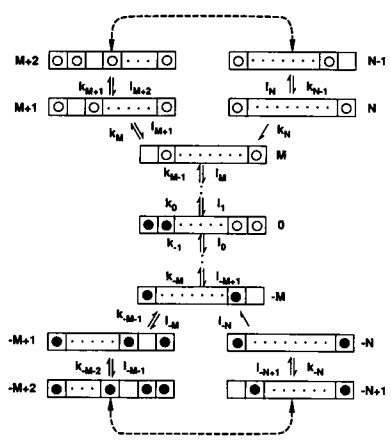


FIGURE 4 State diagram for calculation of the bi-ionic reversal potential. Solid circles represent ions that enter the channel from the inside (*on the left*). Open circles represent ions that enter channels from the outside (*on the right*). The unidirectional flux $\overleftarrow{J}$ is proportional to the probability current flowing from state N to state M. Similarly, $\overrightarrow{J}$ is proportional to the probability current flowing from state $-$N to state $-$M.

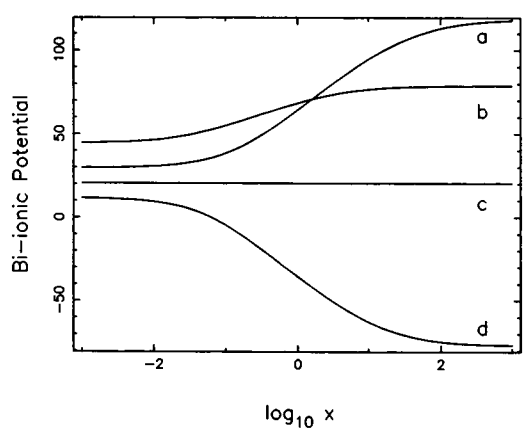


FIGURE 5 Examples of bi-ionic reversal potential as a function of absolute activity $x$. For each case $x_i = x_o = x$. (*a*): $a_i = a_o = 10^8\ s^{-1}\ M^{-1}$, $k_i = 10^7\ s^{-1}$, $k_o = b_i = 10^8\ s^{-1}$, $b_o = 10^7\ s^{-1}$, $n = 2$. (*b*): Same except $n = 4$. (*c*): $a_i = 10^8\ s^{-1}\ M^{-1}$, $a_o = 7 \times 10^8\ s^{-1}\ M^{-1}$, $k_i = 10^8\ s^{-1}$, $k_o = 3.16 \times 10^8\ s^{-1}$, $b_i = 10^7\ s^{-1}$, $b_o = 10^8\ s^{-1}$, $n = 2$. (*d*): $a_i = 10^8\ s^{-1}$, $a_o = 5.0 \times 10^8\ s^{-1}$, $k_i = 10^8\ s^{-1}$, $k_o = b_i = 10^7\ s^{-1}$, $b_o = 10^8\ s^{-1}$, $n = 2$.

the low activity limit and $\overline{V}_R$ in the high activity limit, and in Appendix C we show that $V_R$ either increases or decreases monotonically between those limits. This result is in direct contrast with the prediction of a single-ion model where $V_R$ depends only on the ratio of ion activities $x_i/x_o$ and not on the absolute activities (Läuger, 1973). In the single-vacancy model, $V_R$ is independent of absolute ion activity only in the special case $\underline{V}_R = \overline{V}_R$ (Fig. 5 *c*), that is, when $(n-1)\ln b_o/b_i = n \ln k_o/k_i$. However, it is worth noting that in general, as $n$ becomes large, $\underline{V}_R$ and $\overline{V}_R$ converge to the same value. This means that, for large $n$, the bi-ionic reversal potential of a single-vacancy channel may be difficult to distinguish from that of a single-ion channel.

The expressions given by equations (10) and (11) apply to the simple pore model. A further conclusion can be made, which holds for the reversal potential of a general single vacancy model, because it depends only on the connectivity of the state diagram shown in Fig. 4. The reversal potential does not depend on any specific interactions, e.g., attraction or repulsion, between the i and o ions. This is because all states which include both ions in the pore are found in the linear bridge region connecting the two loops of the diagram. As shown in Appendix D, all such ion interactions cancel out in the calculation of the reversal potential.

A striking feature of certain multi-ion channels, the skeletal muscle $Ca^{2+}$-activated $K^+$ channel in particular, is its strong selectivity favoring the conduction of one ion over others with the same valence and similar size (Blatz and Magleby, 1984; Yellen, 1984; Eisenman et al., 1986). What are the determinants of ion selectivity in a single-vacancy channel? The most frequently used measure of ion selectivity is the permeability ratio measured under bi-ionic conditions. From Nernst–Planck electrodiffusion, the permeability ratio of two ions of the same valence is given by

$$\frac{P_o}{P_i} = \frac{x_i}{x_o} \exp\left(\frac{V_R z e}{k_B T}\right). \tag{12}$$

Eq. 12 is the familiar Goldman–Hodgkin–Katz equation (Goldman, 1943; Hodgkin and Katz, 1949). Although Eq. 12 pertains specifically to Nernst–Planck electrodiffusion, the term on the right side is frequently used as an operational definition of the permeability ratio when experimental data are interpreted. Using Eq. 10, we have for single-vacancy diffusion in the low activity limit:

$$\frac{P_o}{P_i} = \frac{a_o b_o^{(1-n)/n}}{a_i b_i^{(1-n)/n}}. \tag{13}$$

The permeability ratio in the high activity limit is found from Eq. 11:

$$\frac{P_o}{P_i} = \frac{a_o b_o^{-1} k_o^{1/(n-1)}}{a_i b_i^{-1} k_i^{1/(n-1)}}. \tag{14}$$

Thus, in the low-activity limit the permeability ratio is independent of the inner barrier heights. In the high-activity limit the height of the inner barriers is important if $n$ is small. Notice that as $n$ becomes large the low and high activity limits of the permeability ratio become equal and are determined by the ratio of the association and dissociation rate constants. Therefore, as $n$ becomes large it is the binding energy (i.e., the depth of the wells and not the height of the barriers) that determines the permeability ratio in single vacancy conduction: the tighter an ion binds to its sites in the channel, the more permeable it is.

The idea that it is ion binding that determines selectivity is reminiscent of experimental results with $Ca^{2+}$ channels, where selectivity for $Ca^{2+}$ over monovalent ions appears to result from the tighter binding of $Ca^{2+}$ to sites in the conduction pathway (Almers and McCleskey, 1984; Hess and Tsien, 1984; Fukushima and Hagiwara, 1985). These channels have provided the unique opportunity to actually observe $Ca^{2+}$ ions, at micromolar concentrations, block the permeation of monovalent ions. Calcium conduction is observed only after the $Ca^{2+}$ concentration is raised to the millimolar range, when the channel presumably has become "filled" with $Ca^{2+}$ ions. The single vacancy model may reasonably approximate the ion conduction process in $Ca^{2+}$ channels. It would therefore be interesting to compare the affinities of $Ca^{2+}$, $Sr^{2+}$, and $Ba^{2+}$, as determined by their ability to block $Na^+$ conduction through $Ca^{2+}$ channels, with their relative permeabilities measured under bi-ionic conditions (the reversal potential with $Ca^{2+}$ against $Sr^{2+}$ and $Ca^{2+}$ against $Ba^{2+}$, for example).

## FLUX-RATIO EXPONENT

The flux-ratio exponent $n'$ was introduced by Hodgkin and Keynes in their classic work (1955). The exponent describes how the unidirectional flux ratio $\vec{J}/\overleftarrow{J}$ of a permeant ion varies with the ion's electrochemical potential drop across the membrane. This ratio depends on the potential drop according to:

$$\vec{J}/\overleftarrow{J} = \exp\{n' ze(V_0 - V_N)/k_B T\}, \tag{15}$$

where $V_N = (k_B T/ze) \ln (x_o/x_i)$ is the Nernst potential associated with the permeant ion, and the electrochemical potential difference is $ze(V_0 - V_N)$. A measured value of $n' > 1$ is a definitive criterion for multi-ionicity.

We have calculated the flux ratio exponent for the simple pore model from the state diagram shown in Fig. 4, setting $a_i = a_o = a$, $b_i = b_o = b$, and $k_i = k_o = k$. However, Kohler and Heckmann (1979) have already calculated $n'$ for a general single-vacancy channel using a different state diagram, so we will not present our calculations. Our results confirm theirs.

Fig. 6 shows several examples of the flux ratio exponent as a function of absolute activity $x = x_o$. At a fixed value of the electrochemical potential difference, $ze(V_0 - V_N)$, across the membrane, the exponent $n'$ decreases from $n$ at low activity to $n - 1$ at high activity. The range of activities at which the transition from $n' = n$ to $n' = n - 1$ takes place depends on the ratio $a/k$. When the internal hopping rate $k$ is increased by a factor of 10, the curves of Fig. 6 are shifted by one logarithm unit to the right.

The flux ratio exponent depends weakly on $V_0$. In the case $r = x_i/x_o = 20$, with $|V_0 - V_N|$ relatively small, the flux ratio exponent is almost independent of $V_0$. When $r = 0.05$ and $|V_0 - V_N|$ is larger, the voltage dependence of the flux ratio exponent is somewhat more pronounced. As $V_0$ is made more negative, $n'$ decreases at low activities and increases at high activities. Even in the case of $r = 0.05$, the shift in $n'$ may not be resolvable experimentally.

For comparison, the experimental studies of both Begenisich and De Weer as well as Vestergaard-Bogind et al. were performed at negative electrical potential, $V_0 < 0$, and a high ratio of intracellular to extracellular potassium $r > 1$. Studying the $Ca^{2+}$-activated $K^+$ channel of human red blood cells, Vestergaard-Bogind et al. found a nearly constant value of $n' = 2.7$ for a range of transmembrane

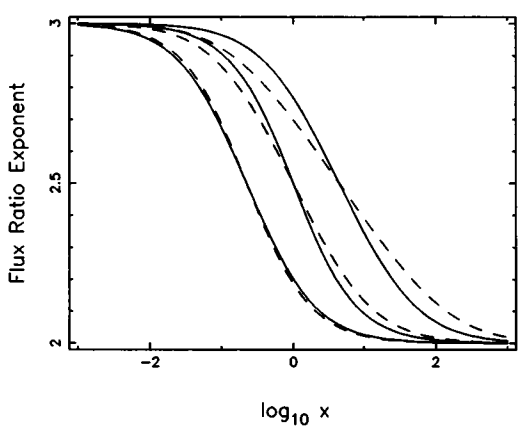


FIGURE 6 Flux ratio exponent as function of activity: $a = 10^8\ s^{-1}\ M^{-1}$, $k = 10^8\ s^{-1}$, $n = 3$ ($n'$ does not depend on $b$). On the abscissa $x = x_o$ is the activity of ions in the outside solution. The three solid curves are calculated for a transmembrane electrical potential of $V_0 = -20$ mV, and activity ratios of $x_i/x_o = 20$, 1, and 0.05 (*left to right*). The corresponding dashed lines show $n'$ calculated for $V_0 = -100$ mV.

potentials and potassium concentrations. Although these authors did not find that $n'$ decreased with increasing $K^+$ concentrations, a drop in $n'$ of 0.1 or 0.2 might have been difficult to resolve. The weak dependence of $n'$ on $V_0$ is consistent with the numerical results of Fig. 6. It would be interesting to see these experiments continued to higher concentrations of intra- and extracellular $K^+$, keeping $|V_0 - V_N|$ as small as possible.

Begenisich and De Weer examined the flux ratio exponent of $K^+$ permeation through the cuttle fish giant axon and found that $n'$ increased as the intracellular $K^+$ concentration was raised. These results suggest that the channel is filling with ions as the $K^+$ activity increases, and probably rules out a single-vacancy conduction mechanism for the delayed-rectifier channel over the concentration range in their experiments.

## SUMMARY

In this paper we have investigated the conduction properties of a hypothetical single-vacancy ion channel. We ask what qualitative properties are expected if an ion channel has only a single vacancy diffusing in its pore, rather than a single ion. The investigation was motivated by recent studies which strongly suggest that $Ca^{2+}$-activated $K^+$ channels from red blood cells and skeletal muscle T-tubules operate as nearly saturated, perhaps single-vacancy pores, over a wide range of experimental conditions (Vestergaard and Bogind, 1985; Neyton and Miller, 1988). A single-vacancy conduction model at first seems to be physically unrealistic because it necessitates the queuing of several ions in a confined space. However, if a $K^+$ channel pore is constructed as a series of electronegative sites (for example, rings of inwardly directed carbonyl oxygens), then the channel may be stable only if most of the sites are occupied by a conducting "counter ion." Viewed in this way, a single-vacancy conduction mechanism is physically plausible, and it may explain recent experimental results with $Ca^{2+}$-activated $K^+$ channels.

The simplicity of the single-vacancy case of multi-ion conduction leads to analytical expressions for several measurable quantities. These expressions enable us to draw general conclusions about single-vacancy conduction, which we now summarize. First, we have found that single-vacancy conduction, like many other multi-ion conduction models (for example, Hille and Schwarz, 1978; Urban and Hladky, 1979) predicts a maximum in the conductance-concentration relationship. For single-vacancy conduction, the maximum is expressed very simply as a quadratic term in the denominator. Furthermore, we have shown that single-vacancy conduction

models do not always yield an experimentally accessible maximum. Second, we have shown that the reversal potential under bi-ionic conditions is generally a function of the absolute ion concentration $x$, although conditions exist where $V_R$ may be independent of $x$. In particular, as the number of sites $n$ (and thus the number of ions) increases, a weaker dependence of $V_R$ on $x$ is expected. Therefore, as $n$ increases, $V_R(x)$ for single-vacancy conduction becomes more like that for single-ion conduction. Finally, we have found conditions where the permeability ratio depends only on ion *binding*. Specifically, as $n$ increases ion binding becomes the major determinant in the permeability ratio.

## APPENDIX A

Knowledge of the King–Altman method (1956) is assumed. A very clear and concise description is presented by Plowman (1972). Hill has extended the method to include the efficient calculation of cycle fluxes (1977).

The flux $J$ is given by Eq. 1, where the denominator $D$ is the sum of directional diagrams $D_m$:

$$D = \sum_{m=0}^{n} D_m, \quad \text{where } D_m = \sum_{h=1}^{n+1} \prod_{i=1}^{h-1} l_{i+m} \prod_{j=h}^{n} k_{j+m}. \tag{A1}$$

Rate constant indices are interpreted mod $(n+1)$. If the upper index over a product symbol is less than the lower index, the product is taken to be unity. The $l_i$ and $k_j$ are given by Eq. 3. Inserting these into Eq. A1 and expanding, obtain:

$$D_0 = k^{n-2} \cdot \left\{ x_o a k e^{-n\nu} + x_i x_o a^2 \sum_{g=-n+2,n-2,2} e^{g\nu} + x_i a k e^{n\nu} \right\}, \tag{A2}$$

$$D_1 = k^{n-2} b \left\{ k e^{-n\nu} + k e^{-(n-2)\nu} + x_i a \sum_{g=-n+4,n,2} e^{g\nu} \right\}, \tag{A3}$$

$$D_n = k^{n-2} b \left\{ x_o a \sum_{g=-n,n-4,2} e^{g\nu} + k e^{(n-2)\nu} + k e^{n\nu} \right\}, \tag{A4}$$

$$D_m = k^{n-2} b \left\{ x_o a \sum_{g=-n,-n-4+2m,2} e^{g\nu} + k e^{(-n-2+2m)\nu} + k e^{(-n+2m)\nu} + x_i a \sum_{g=-n+2m+2,n,2} e^{g\nu} \right\}. \tag{A5}$$

In the last equation $2 \le m \le n-1$. The notation under the summation signs means that the index g ranges from the first argument to the second argument in steps of 2. Set $x_i = x_o = x$ and gather coefficients of $e^{m\nu}$ to find:

$$J = D^{-1} a k b x [e^{(n+1)\nu} - e^{-(n+1)\nu}], \tag{A6}$$

where

$$D = [xak + kb + (n-1)xab](e^{-n\nu} + e^{n\nu}) + [x^2a^2 + 2kb + (n-2)xab] \sum_{g=-n+2,n-2,2} e^{g\nu}. \tag{A7}$$

the sum of Eq. A7 can be simplified by making use of the identity

$$\sum_{g=-n+2,n-2,2} e^{g\nu} = \frac{\sinh(n-1)\nu}{\sinh\nu}, \tag{A8}$$

leading directly to Eq. 4.

## APPENDIX B

Refer to the bi-ionic state diagram in Fig. 4. The unidirectional fluxed $\overleftarrow{J}$ and $\overrightarrow{J}$ are given by

$$\overleftarrow{J} = D^{-1} D_N k_N \quad \text{and} \quad \overrightarrow{J} = D^{-1} D_{-N} l_{-N}, \tag{B1}$$

where $D_m$ is the directional diagram for state m and $D = \Sigma D_m$. Only $D_N$ and $D_{-N}$ need be explicitly evaluated. These are given by:

$$D_N = \overline{Q} \prod_{i=-M}^{N-1} k_i \text{ with } \overline{Q} = \sum_{s=M}^{N} \prod_{q=M+1}^{s} k_{-q} \prod_{r=s+1}^{N} l_{-r}, \tag{B2}$$

and

$$D_{-N} = Q \prod_{i=-N+1}^{M} l_i \quad \text{with} \quad Q = \sum_{s=M}^{N} \prod_{q=M+1}^{s} l_q \prod_{r=s+1}^{N} k_r. \tag{B3}$$

Note that $M = \frac{1}{2}(n-1)n$ and $N = \frac{1}{2}n(n+1)$. Counting carefully, one evaluates:

$$\prod_{i=-M}^{N} k_i = x_o^n a_o^n k_i^{(n-2)(n-1)/2} k_o^{(n-1)n/2} b_i^{n-1} b_o e^{-(n^2+1)\nu}, \tag{B4}$$

$$\prod_{i=-N}^{M} l_i = x_i^n a_i^n k_i^{(n-1)n/2} k_o^{(n-2)(n-1)/2} b_i b_o^{n-1} e^{(n^2+1)\nu}, \tag{B5}$$

$$Q = k_o^{n-2} b_o \left\{ x_o a_o \sum_{g=-n,n-4,2} e^{g\nu} + k_o e^{(n-2)\nu} + k_o e^{n\nu} \right\}, \tag{B6}$$

$$\overline{Q} = k_i^{n-2} b_i \left\{ k_i e^{-n\nu} + k_i e^{-(n-2)\nu} + x_i a_i \sum_{g=-n+4,n,2} e^{g\nu} \right\}. \tag{B7}$$

Putting all of these results together, we have expressions for $D\overleftarrow{J}$ and $D\overrightarrow{J}$. Note that $D\overleftarrow{J}$ is a decreasing function of $V_0$ because the term $\exp[-(n^2+1)\nu]$ in Eq. B4 dominates the exponentials in Eq. B7. Similarly, $D\overrightarrow{J}$ is an increasing function of $V_0$. The two unidirectional currents are equal at a unique value of $V_R$.

The low activity limit $\underline{V}_R$ is obtained from $\overleftarrow{J}(V_R) = \overrightarrow{J}(V_R)$ by neglecting the terms proportional to $x_i a_i$ and $x_o a_o$ in $Q$ and $\overline{Q}$. Conversely, the high activity limit $\overline{V}_R$ is obtained by neglecting the terms proportional to $k_o$ and $k_i$ in the braces of Eqs. B6 and B7.

## APPENDIX C

In this appendix we prove that the bi-ionic reversal potential $V_R$ for single-vacancy diffusion is a monotonic function of the absolute concen-

tration $x$, except when $V_R$ does not depend on $x$ at all. Consider the function:

$$\mathcal{F}(V_R(x), x) = \ln \frac{\overleftarrow{J}(V_R(x), x)}{\overrightarrow{J}(V_R(x), x)} \equiv 0. \quad \text{(C1)}$$

The function $\mathcal{F}$ is identically zero because $\overleftarrow{J}(V_R(x), x) = \overrightarrow{J}(V_R(x), x)$ by definition of $V_R$. Differentiating $\mathcal{F}$ with respect to $x$ we find:

$$\frac{dV_R}{dx} = -\frac{\partial \mathcal{F}/\partial x}{\partial \mathcal{F}/\partial V_R}. \quad \text{(C2)}$$

It is easy to see that $\partial \mathcal{F}/\partial V_R$ is finite and strictly negative for all $x$. $D\overleftarrow{J}$ is a positive sum of decreasing exponentials and decreases monotonically and with finite slope as $V_0$ increases. Similarly, $D\overrightarrow{J}$ is a positive sum of increasing exponentials and increases monotonically and with finite slope as $V_0$ increases. Therefore, the ratio $\overleftarrow{J}/\overrightarrow{J}$ is positive and decreasing with finite slope for all finite $V_0$, and so the logarithm of the ratio decreases with finite slope. It follows that the zeros of $dV_R/dx$ are identical with those of $\partial \mathcal{F}/\partial x$.

Writing out $\mathcal{F}$ we have

$$\mathcal{F}(V_R(x), x) = -n \ln r + n \ln \frac{a_o}{a_i} + \ln \frac{k_o}{k_i} + (n-1) \ln \frac{b_i}{b_o} - 2(n^2+1)\nu + \ln \left\{ \frac{k_i e^{-n\nu} + k_i e^{-(n-2)\nu} + rxa_i \sum_{g=-n+4,n,2} e^{g\nu}}{xa_o \sum_{g=-n,n-4,2} e^{g\nu} + k_o e^{(n-2)\nu} + k_o e^{n\nu}} \right\}. \quad \text{(C3)}$$

where $x = x_o$, $r = x_i/x_o$ and for this appendix we define $\nu = eV_R/2(n+1)k_BT$. $\mathcal{F}$ depends on $x$ only through the argument of the logarithm. Because that argument is strictly positive and finite, it follows that:

$$\frac{\partial \mathcal{F}}{\partial x} = 0 \longleftrightarrow \frac{\partial}{\partial x} \left\{ \frac{k_i e^{-n\nu} + k_i e^{-(n-2)\nu} + rxa_i \sum_{g=-n+4,n,2} e^{g\nu}}{xa_o \sum_{g=-n,n-4,2} e^{g\nu} + k_o e^{(n-2)\nu} + k_o e^{n\nu}} \right\} = 0. \quad \text{(C4)}$$

The expression in braces has the form $(E + Fx)/(G + Hx)$, where $E$, $F$, $G$, and $H$ do not depend on $x$. Differentiating, one finds that the derivative is equal to zero only when $FG = EH$. Substituting from Eq. C4 the appropriate expressions for $E$, $F$, $G$, and $H$ we find:

$$\frac{dV_R}{dx} = 0 \longleftrightarrow V_R = V_R^* = \frac{k_BT}{ze} \left\{ \ln \frac{x_o}{x_i} + \ln \frac{a_o}{a_i} - \ln \frac{k_o}{k_i} \right\}. \quad \text{(C5)}$$

Combining Eq. C5 with $\underline{V}_R$ and $\overline{V}_R$ defined in (10) and (11), we can show:

$$(\overline{V}_R - V_R^*)(V_R^* - \underline{V}_R) = -\frac{n}{n-1} \left( \frac{k_BT}{ze} \right)^2 \left\{ \ln \frac{k_o}{k_i} - \frac{n-1}{n} \ln \frac{b_o}{b_i} \right\}^2. \quad \text{(C6)}$$

The right hand side is strictly negative unless the expression in braces is zero. When it is negative it follows that $V_R^*$ cannot be contained in the interval $[\underline{V}_R, \overline{V}_R]$ (alternately, $[\overline{V}_R, \underline{V}_R]$) and $V_R(x)$ must be monotonic. When the expression in braces is zero, $\underline{V}_R = V_R^* = \overline{V}_R$ and the reversal potential is independent of the absolute concentration.

## APPENDIX D

The reversal potential of the single-vacancy model does not depend on any specific interactions between the two permeant ions. The potential $V_R$ is in general implicitly defined by $\overleftarrow{J}(V_R) = \overrightarrow{J}(V_R)$. All interactions between ions i and o are confined to the bridge region connecting the two loops of Fig. 4. These interactions enter the implicit equation only via the ratio of rate constants:

$$\mathcal{B} = \frac{k_{-M} \times \cdots \times k_{-1} k_0 \times \cdots \times k_{M-1}}{1_{-M+1} \times \cdots \times 1_0 1_1 \times \cdots \times 1_M}. \quad \text{(D1)}$$

We now use an argument very similar to one given by Kohler and Heckmann in their calculation of cyclic products of rate constants (1979). According to absolute rate theory, a rate constant $k_i$ corresponding to internal hopping over a barrier or exit from a channel would have the general form:

$$k_i = \kappa \exp - [g(i, i+1) - g(i)]. \quad \text{(D2)}$$

A rate constant $k_i$ corresponding to entrance into the channel from the inside ($z$ = i) or outside ($z$ = o) solution has the form:

$$k_i = \kappa \exp - [g(i, i+1) - g(i) - \mu_z]. \quad \text{(D3)}$$

In these expressions $\kappa = k_BT/h$ is a frequency factor involving Planck's constant $h$. The symbol $g(i)$ denotes the dimensionless standard free energy of the pore in state i. Similarly, $g(i, i+1)$ is the dimensionless standard free energy of the pore in the transition state between i and i + 1. Analogous expressions may be developed for the $l_i$, substituting i − 1 for i + 1 in Eqs. D2 and D3. The symbols $\mu_o$ and $\mu_i$ correspond to the electrochemical potentials of the ions o and i in the outer and inner reservoirs, respectively.

Substituting Eqs. D2 and D3 and the corresponding expressions for the $l_i$ into Eq. D1 we find:

$$\mathcal{B} = \exp [g(-M) - g(M)] \exp [(n-1)(\mu_o - \mu_i)]. \quad \text{(D4)}$$

The ratio $\mathcal{B}$ depends only on the states −M and M, in which only a single type of ion occupies the channel, as well as the chemical potentials $\mu_o$ and $\mu_i$. Because $V_R$ depends on the bridge states only through $\mathcal{B}$, the reversal potential is independent of any specific interactions between the two types of ions.

The applicability of absolute rate theory to channel models has recently been challenged (Cooper et al., 1988). However, those authors also conclude that Kramer's approximation to diffusion over a potential barrier is satisfactory when the height of the barrier is at least several $k_BT$ and the potential profile provides clearly defined binding sites. We have made a similar analysis of $\mathcal{B}$ using Kramer's approximation. The exponential dependence of the rate constants on free energies remains the same as shown in Eqs. D2 and D3, but the prefactors become more complicated. Nevertheless, all dependence on intermediate states cancels out in the ratio, and we again conclude that the reversal potential is independent of any specific interaction between the two ions.

We gratefully acknowledge stimulating discussions with Irving Epstein and Peter Jordan and thank Christopher Miller for a critical review of this manuscript. Bruce Clarke introduced us to the King–Altman method. We thank A. A. Lev for pointing out to us the important paper by Kohler and Heckmann.

M. Schumaker was supported by National Science Foundation grant DMB-8604794 to Irving Epstein.

*Received for publication 24 January 1990 and in final form 25 May 1990.*

## REFERENCES

Almers, W., and E. W. McCleskey. 1984. The non-selective conductance in calcium channels of frog muscle: calcium selectivity in a single-file pore. *J. Physiol. (Lond.)*. 353:585–608.

Begenisich, T. B., and P. De Weer. 1980. Potassium flux ratio in voltage-clamped squid giant axons. *J. Gen. Physiol.* 76:83–98.

Blatz, A., and K. Magleby. 1984. Ion conductance and selectivity of single calcium-activated potassium channels in cultured rat muscle. *J. Gen. Physiol.* 84:1–23.

Cahalan, M. D., and T. B. Begenisich. 1976. Sodium channel selectivity: dependence of internal permeant ion concentration. *J. Gen. Physiol.* 68:11–125.

Chandler, W. K., and H. Meues. 1965. Voltage clamp experiments on internally perfused giant axons. *J. Physiol. (Lond.)*. 180:788–820.

Cooper, K. E., P. Y. Gates, and R. S. Eisenberg. 1988. Diffusion theory and discrete rate constants in ion permeation. *J. Membr. Biol.* 106:95–105.

Eisenman, G., R. Latorre, and C. Miller. 1986. Multi-ion conduction and selectivity in the high-conductance $Ca^{++}$-activated $K^+$ channel from skeletal muscle. *Biophys. J.* 50:1025–1034.

Finkelstein, A., and O. S. Andersen. 1981. The gramicidin A channel: a review of its permeability characteristics with special reference to the single-file aspect of transport. *J. Membr. Biol.* 59:155–171.

Fukushima, Y., and S. Hagiwara. 1985. Currents carried by monovalent cations through calcium channels in mouse neoplastic B lymphocytes. *J. Physiol. (Lond.)*. 358:255–284.

Gárdos, G. 1958. The function of calcium in the potassium permeability of human erythrocytes. *Biochim. Biophys. Acta.* 30:653–654.

Goldman, D. E. 1943. Potential, impedance and rectification in membranes. *J. Gen. Physiol.* 27:37–60.

Hess, P., and R. W. Tsien. 1984. Mechanism of ion permeation through calcium channels. *Nature (Lond.)*. 309:453–456.

Hill, T. L. 1977. Free Energy Transduction in Biology. Academic Press, New York. 229 pp.

Hille, B., and W. Schwarz. 1978. Potassium channels as multi-ion single-file pores. *J. Gen. Physiol.* 72:409–442.

Hodgkin, A. L., and B. Katz. 1949. The effect of sodium ions on the electrical activity of the giant axons of the squid. *J. Physiol. (Lond.)*. 108:37–77.

Hodgkin, A. L., and R. D. Keynes. 1955. The potassium permeability of a giant nerve fiber. *J. Physiol. (Lond.)*. 128:61–88.

Horowicz, P., P. W. Gage, and R. S. Eisenberg. 1968. The role of the electrochemical gradient in determining potassium fluxes in frog striated muscle. *J. Gen. Physiol.* 51:193s–203s.

King, E. L., and C. Altman. 1956. A schematic method of deriving the rate laws for enzyme-catalyzed reactions. *J. Phys. Chem.* 60:1375–1378.

Kohler, H.-H., and K. Heckmann. 1979. Unidirectional fluxes in saturated single file pores of biological and artificial membranes I. Pores containing no more than one vacancy. *J. Theor. Biol.* 79:381–401.

Läuger, P. 1973. Ion transport through pores: a rate-theory analysis. *Biochim. Biophys. Acta.* 311:423–441.

Levitt, D. G. 1986. Interpretation of biological ion channel flux data: reaction rate versus continuum theory. *Annu. Rev. Biophys. Biophys. Chem.* 15:29–57.

Neyton, J., and C. Miller. 1988. Discrete $Ba^{2+}$ block as a probe of ion occupancy and pore structure in the high-conductance $Ca^{2+}$-activated $K^+$ channel. *J. Gen. Physiol.* 92:569–586.

Plowman, K. M. 1972. Enzyme Kinetics. McGraw-Hill Inc., New York. 171 pp.

Spalding, B. C., O. Senyk, J. G. Swift, and P. Horowicz. 1981. Unidirectional flux ratio for potassium ions in depolarized frog skeletal muscle. *Am. J. Physiol.* 241:c68–c75.

Urban, B. W., and S. B. Hladky. 1979. Ion transport in the simplest single file pore. *Biochim. Biophys. Acta.* 554:410–429.

Urban, B. W., S. B. Hladky, and D. A. Haydon. 1978. The kinetics of ion movements in the gramacidin channel. *Fed. Proc.* 37:2628–2632.

Vestergaard-Bogind, B., P. Stampe, and P. Christophersen. 1985. Single-file diffusion through the $Ca^{2+}$-activated $K^+$ channel of human red blood cells. *J. Membr. Biol.* 88:67–75.

Villarroel, A., O. Alvarez, and G. Eisenman. 1988. A maximum in conductance occurs for the large $Ca^{2+}$-activated $K^+$ channel at high $Rb^+$ concentration. *Biophys. J.* 53:259a.

Yellen, G. 1984. Ionic permeation and blockade in $Ca^{2+}$-activated $K^+$ channels of bovine chromaffin cells. *J. Gen. Physiol.* 84:157–186.